Title

Uptake of water by an acid-base nanoparticle: theoretical and experimental studies of the methanesulfonic acid-methylamine system.

Journal

Physical chemistry chemical physics : PCCP, 20(34)

ISSN

1463-9076

Authors

Xu, Jing
Perraud, Véronique
Finlayson-Pitts, Barbara J
et al.

Publication Date

2018-08-01

DOI

10.1039/c8cp03634a

PCCP

PAPER

View Article Online
View Journal | View Issue

Cite this: *Phys. Chem. Chem. Phys.*, 2018, **20**, 22249

Uptake of water by an acid–base nanoparticle: theoretical and experimental studies of the methanesulfonic acid–methylamine system†

Jing Xu, [a] Véronique Perraud, [a] Barbara J. Finlayson-Pitts *[a] and R. Benny Gerber *[ab]

The effect of water on the growth of dry nano-size acid–base particles is not yet known. In this paper, we investigate the uptake of water by nano-size particles composed of methanesulfonic acid (MSA) and methylamine (MA) using a combination of quantum chemical calculations and laboratory experiments. Calculations were performed on the $(MSA–MA)_4$ cluster as the dry nanoparticle model, which forms a pseudo-cubic structure, to which twelve water molecules were added successively. Theoretical results show that the hydrated clusters $(MSA–MA)_4–(H_2O)_n$, n = 1 to 12 are thermodynamically stable. In *ab initio* dynamic simulations, no loss of water or significant changes of structure are seen for at least 10 picoseconds. In all the clusters studied, most of the water molecules lie on the face of the $(MSA–MA)_4$ initial dry unit, and water is found to be incorporated inside the initial unit for n ranging from five to twelve. Sizes of hydrated clusters exceed significantly that of the dry cluster only for $n \geq 6$. These theoretical results suggest that dry MSA–MA clusters cannot dissociate in small quantities of water. Calculations of hydrated cluster distributions at steady state show that the cluster compositions studied, with up to 12 water molecules, encompass all the hydrated clusters under the experimental conditions (RH ~ 19%, 300 K). Experiments performed in a glass flow reactor showed no changes in size or number concentration when particles formed from MSA–MA were subsequently exposed to water vapor, in contrast to increases in both size and number when water was present during particle formation. Thus, the results seem to imply for both experiment and theory that growth in size of a particle due to uptake of water requires the previous presence of some level of hydration. These results illustrate the importance for atmospheric models of understanding on a molecular basis the mechanisms of particle formation in air.

Received 8th June 2018,
Accepted 11th August 2018

DOI: 10.1039/c8cp03634a

rsc.li/pccp

Introduction

Atmospheric particles are well-known for their negative effects on climate[1,2] and human health.[3–5] Acid–base particles are a common class of atmospheric particles and have received increasing attention.[6–8] Sulphuric acid (H_2SO_4) has been identified as a key component in atmospheric particles.[9–11] Numerous experimental studies have shown that bases, *e.g.*, ammonia or amines, can enhance new particle formation compared to the binary system $H_2SO_4–H_2O$,[11–16] in agreement with theoretical calculations that acid–base clusters are more stable than hydrated H_2SO_4 clusters.[17–25] In addition to the well-known H_2SO_4, methanesulfonic acid ($CH_3S(O)(O)OH$, MSA) is another important sulfur-containing acid in the atmosphere.[26–36] The concentrations of gaseous MSA in the atmosphere are in the range of $\sim 10^5–10^7$ molecules cm^{-3} (corresponding to 10–100% of that of H_2SO_4),[36–38] which can drive new particle formation (NPF) in air.[39] The formation of particles involving MSA and ammonia/amines in the presence and absence of water have been previously explored in laboratory studies,[39–45] and corresponding quantum chemical calculations on MSA-based clusters were also carried out.[39–42,45–54] However, compared to H_2SO_4, the studies on MSA are still very limited.

There is a lot of evidence that the presence of water has a significant effect on NPF from both MSA and H_2SO_4.[6,7,11–14,39–43,55–58] For example, laboratory measurements show that the formation of MSA–amine particles are more efficient in the presence of water vapor, and particle number concentrations and size distributions both increase as the relative humidity increases.[39–43] Computational studies also suggest that the presence of water leads to a higher

[a] *Department of Chemistry, University of California, Irvine, CA 92697, USA. E-mail: bjfinlay@uci.edu; Fax: +1-(949)-824-2420; Tel: +1-(949)-824-7670*
[b] *Institute of Chemistry, Fritz Haber Research Center, Hebrew University of Jerusalem, Jerusalem 91904, Israel. E-mail: benny@fh.huji.ac.il*

† Electronic supplementary information (ESI) available. See DOI: 10.1039/c8cp03634a

particle formation rate compared to the dry case.[59,60] Quantum chemical calculations indicate that water can facilitate proton transfer from the acid to the base,[18,20,46,47,60–65] stabilize the acid–base clusters,[17,18,22,47,64] and reduce the reaction barrier.[66] Most of these studies show the effect of water in the initial step of NPF, while the role of water uptake on particles already present remains uncertain.

Methylamine (CH_3NH_2, MA) is an amine commonly found in the atmosphere.[67–69] Earlier studies demonstrated that MSA combines efficiently with MA to form nanoparticles,[41,43,44] and the structures of the corresponding nano-size low-energy anhydrous MSA–MA clusters were reported in a previous study.[48] Inspired by this, the objectives in this paper can be described as follows: (1) What is the effect of added water molecules on the size and other properties of dry nanoparticles composed of MSA and MA? (2) Connected with this, what is the stability of the MSA–MA nanoparticles with respect to the addition of water?

We report here a combined theoretical and experimental investigation of the uptake of water by pre-existing MSA–MA nanoparticles. For the theoretical calculations, a cage-like $(MSA–MA)_4$ cluster was chosen as the model of a nano-size acid–base particle. A previous study predicted that this cluster has a very high thermodynamic and dynamic stability and can be seen as an important intermediate in the formation and growth of MSA–MA particles.[48] Calculations examine how this initial cluster behaves in presence of increasing numbers of water molecules ranging from one to twelve, where the clusters are calculated using density functional theory and *ab initio* molecular dynamics. Energetics, structures and dynamics of these hydrated clusters are also reported. Experiments carried out in a glass flow reactor where MSA reacts with MA under dry conditions, and subsequently exposed to water vapor are presented in support of the calculations.

Theoretical methods

The initial structures for the $(MSA–MA)_4–(H_2O)_n$ (n = 1 to 12) clusters were obtained by gradually adding water molecules to the stable cage-like $(MSA–MA)_4$ anhydrous cluster. In previous study,[48] more than three hundred initial structures of clusters composed of four MSA and four MA were generated randomly using PACKMOL package. Upon optimization, the cage-like $(MSA–MA)_4$ still has the lowest energy among all local minima computed. The next lowest in energy conformer is higher by 4.71 kcal mol^{-1} than the cage structure, and quickly converts to the latter in room temperature molecular dynamics simulations. Hence, the cage-like $(MSA–MA)_4$ can be seen as the global minimum, and is a reasonable model for this study. Because the 3-D skeleton of the $(MSA–MA)_4$ initial cluster looks like a cube, the probable locations of the added water molecules we considered here are 'on the face of' or 'inside' the $(MSA–MA)_4$ unit, respectively. The geometry of the most stable $(MSA–MA)_4$ unit defined from our previous study was used as the starting anhydrous structure.[48] In order to consider possible local minima, PACKMOL package was employed to generate initial structures. Optimization, frequency, and energy calculations for these nanoclusters were performed using the BLYP-D[70,71]/6-31+G(d) method.[72,73] In order to verify the credibility of the small basis set, more costly basis sets such as aug-cc-pVDZ[74] and 6-311++G(3df,3dp)[75] were used for our test calculations on three low-lying isomers of the smallest cluster $(MSA–MA)_4–H_2O$. The locations of water molecules in the three isomers are (1) on the face of the $(MSA–MA)_4$ cluster, binding with two deprotonated MSA (MSA^-) and one protonated MA (H^+MA); (2) on the face of the $(MSA–MA)_4$ cluster, binding with two MSA^-; and (3) inside of the $(MSA–MA)_4$ unit, binding with two MSA^-, respectively. In addition, the three isomers were also calculated using the B3LYP-D3[71,76,77]/aug-cc-pVDZ method, which has been tested on MSA–MA and is in agreement with MP2 and CCSD(T) results in a previous study.[47] Fig. S1 (ESI†) shows the corresponding structures and the relative energies of the three isomers at the levels of BLYP-D/6-31+G(d), BLYP-D/aug-cc-pVDZ, BLYP-D/6-311++G(3df,3dp) and B3LYP-D3/aug-cc-pVDZ. All the energies have been corrected with zero-point energies. The test results showed similar structures and relative energies at the four levels of theory. Hence, the less time-consuming BLYP-D/6-31+G(d) is considered to be sufficient to predict qualitatively the lowest-energy isomer for the nano-size clusters investigated in the present study. In order to compare the charge distributions of hydrated and anhydrous clusters, natural bond orbital (NBO) analysis was used to calculate partial charges (δ).[78,79]

Molecular dynamic (MD) simulations are usually used to verify the dynamic stability at various temperatures. The dynamic stability we intended here is relevant to processes such as structural rearrangements of the hydrated clusters and to proton transfer rates within these small particles, which may yield different results compared to quantum chemical calculations performed at 0 K. Hence, Born–Oppenheimer molecular dynamics (BOMD) simulations were carried out on each hydrated cluster at T = 300 K for 10 picoseconds (ps) using the BLYP-D/6-31+G(d) potential on-the-fly method. The time step used was 0.48 femtosecond (fs). All calculations in this paper were performed using the Q-CHEM 4.3 program package.[80]

In order to study the hydrate distribution, simulations of steady-state concentrations of clusters were performed using the Atmospheric Cluster Dynamic Code (ACDC).[81] We used $(MSA–MA)_4$ and H_2O as the monomers to simulate the concentrations of hydrated clusters. For simulating the experimental conditions, we assumed that the concentrations of $(MSA–MA)_4$ and water were 10^6 and 10^{17} (RH = 19%) molecules cm^{-3}, respectively. Note that no external sinks, *e.g.*, coagulation scavenging or wall and dilution losses, were considered here.

Experimental methods

Experiments were performed using a custom-built 1-m borosilicate glass aerosol flow reactor described in detail elsewhere.[42,43,82] The flow reactor was equipped with three fixed perforated ring inlets at the upstream end and three perforated spoke inlets that are movable as a unit to change the reaction time between the rings and spokes, and spokes and sampling tube. The six ports allow the

addition of reactants separately at different points (see Fig. S2, ESI†). The sequence of addition was the following: 10 L min^{-1} of clean dry clean air was injected in the first ring (ring A); MSA ($\sim$0.2 L min^{-1}) mixed in with 1.8 L min^{-1} of air was added through the second ring (ring B); MA ($\sim$0.17 L min^{-1}) mixed in with 0.83 L min^{-1} of air was added through the third ring (ring C) facing backward; 3 L min^{-1} of air was added through the second spoke (spoke 2); no air flow was introduced *via* the first or last spoke inlets (spoke 1 and 3 respectively). The total flow rate under those conditions was 16 L min^{-1} and the reaction times along the length of the reactor were determined using a conversion factor of 0.132 s cm^{-1} based upon previous measurements.[82] All flows were controlled by high-precision mass flow controllers (Alicat or MKS) and were checked with a flow meter (Gilibrator 2, Sensidyne) prior to each experiment. For experiments performed under humid conditions (RH 18–19%), water vapor generated by passing 3 L min^{-1} of air through a bubbler maintained at room temperature was added either through the second spoke (replacing the 3 L min^{-1} of dry air), *i.e.*, after the formation of the MSA–MA particles; or through the first ring (ring A), *i.e.*, with MSA reacting with MA and water at the same time (adjustment of the air flow was then made to maintained a total of 10 L min^{-1} through the ring). For all experiments performed, spoke 2 was located 62 cm downstream from ring B, giving a reaction time for MSA with MA corresponding to a reaction time of $\sim$8.2 s (taking ring B as t = 0 s) before water was added at the spokes. The air used throughout the experiments was dry clean air generated from a purge air generator (model 75–62, Parker-Balston) which was further purified using carbon/alumina media (Perma Pure, LLC) and a 0.1 μm filter (DIF-N70; Headline Filters). In addition, the air introduced at the first ring (ring A; 10 L min^{-1} or 7 L min^{-1}) was also passed through a cartridge containing phosphoric acid (ACS grade, EMD) coated glass beads to minimize contaminant ammonia that might be present in purge air prior to its introduction into the flow reactor. All experiments were performed at atmospheric pressure and 296 K. Particle number concentrations and size distributions were measured using a moveable stainless steel sampling line located inside the flow reactor. The interaction time for water added through the spokes with the preformed MSA–MA particles was 5.7 s up to the entrance of the sampling line.

Methanesulfonic acid was generated in the gas phase by passing dry purge air over the pure liquid (Sigma-Aldrich, $\geq$99%) maintained at room temperature in a glass trap. The concentration of MSA exiting the trap was measured regularly by collecting the entire flow of MSA onto a 0.45 μm Durapore filter (Millex-HV) for 10 min and subsequent extraction with 10 mL of nanopure water (18.2 mΩ cm; model 7146; Thermo Scientific, Barnstead). The extracts were then analyzed by ultra performance liquid chromatography electrospray mass spectrometry (Quattro Premier XE, Waters) using a multiple reaction monitoring method (MRM, transition m/z 95 $\rightarrow$ m/z 80). The concentration of MSA from the trap was 427 $\pm$ 39 ppb (1 standard deviation, calculated from multiple samples taken over time). The flow reactor was conditioned with MSA for approximately two days prior to experiments to passivate the wall of the inlet and the reactor.

Gas phase MA was generated using a commercially available permeation tube (VICI Metronics) containing the pure liquid enclosed inside a U-shaped glass tube immersed in a water bath to maintain the temperature at 293 K. Purge air at 0.17 L min^{-1} flowed through the glass tube to generate gas phase MA. The concentration of MA was measured regularly by ion chromatography (Dionex ICS 1100). Collection of the gas phase amine was performed using a custom-made cation ion exchange resin[83] for 20 min at a flow rate of $\sim$0.11 L min^{-1} and subsequent extraction with 10 mL of the IC eluent (0.05 M oxalic acid in 18.2 mΩ cm water). The eluent was made every day by diluting a concentrated commercial oxalic acid solution (0.5 M, Fluka) with 18.2 mΩ cm water. Three successive extractions of the same cartridge were carried out and summed up to yield the total concentration produced by the permeation tube. No quantifiable ammonia or other contaminant was observed from the MA permeation tube and the concentration of MA measured out of the permeation tube was 122 $\pm$ 5 ppb (1 standard deviation estimated from the analysis of 3 replicates).

The concentrations reported hereafter for both MSA and MA in the flow reactor are upper limits as both compounds are sticky and may be lost on the walls of the inlets and the reactor, even after extensive conditioning. The relative humidity inside the flow tube was measured using a Vaisala RH probe (HMT 838, Vaisala). Particle size distributions were measured at 13.9 s reaction time relative to ring B. For experiments where H_2O was added at spoke 2, this time includes 8.2 s for particles to form from MSA and MA, and 5.7 s of interaction time of the preformed particles with water. A scanning mobility particle sizer (SMPS model 3936, TSI) equipped with a TSI 3080 classifier, a nano-differential mobility analyzer (model 3085, TSI), a butanol-based condensation particle counter (model 3776, TSI), a ^{210}Po neutralizer (model 2021, NRD) and a 0.071 cm impactor nozzle was used for these measurements. Sheath air flow was 15 L min^{-1} and the aerosol flow was 1.5 L min^{-1}. The cut-off diameter under those conditions is stated to be 2.5 nm by the manufacturer based on sucrose particles. In all experiments, the flow reactor was conditioned with the last reactant added for 2 hours prior to making measurements.

Results and discussion

Locations of water molecules

The nano-size $(MSA–MA)_4$ cluster was first optimized at the level of BLYP-D/6-31+G(d). The resulting structure is consistent with our previous study,[48] *i.e.*, a closed cage-like structure composed of four ion pairs (MSA^-–H^+MA), with an average bond length of the hydrogen bonds of 1.81 Å (Fig. S3, ESI†). Twelve water molecules were then added to the $(MSA–MA)_4$ cluster sequentially. The most stable structures of $(MSA–MA)_4$–$(H_2O)_n$, n = 1 to 12 are shown in Fig. 1.

Clusters with n = 1, 2, 5 and 11 are chosen as representative clusters and are shown in Fig. 2. There are two distinct types of structures, with subsets within each. In the first type, water resides on the face of the cluster (Fig. 2a and b) while in the

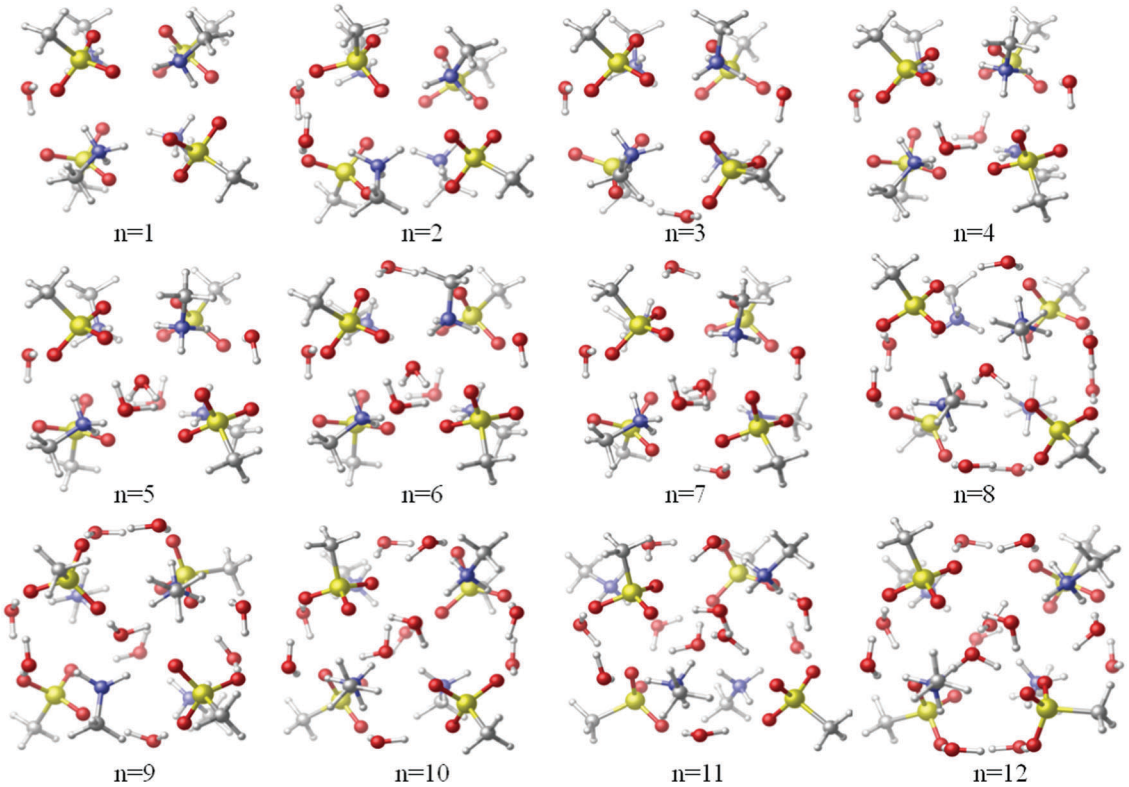

Fig. 1 Structures of $(MSA–MA)_4–(H_2O)_n$, n = 1 to 12. Yellow, red, blue, gray and white spheres represent sulfur, oxygen, nitrogen, carbon and hydrogen atoms, respectively. For a better view, all the hydrogen bonds between oxygen and hydrogen are omitted, and the molecules located on the inside of the unit cell are blurred out.

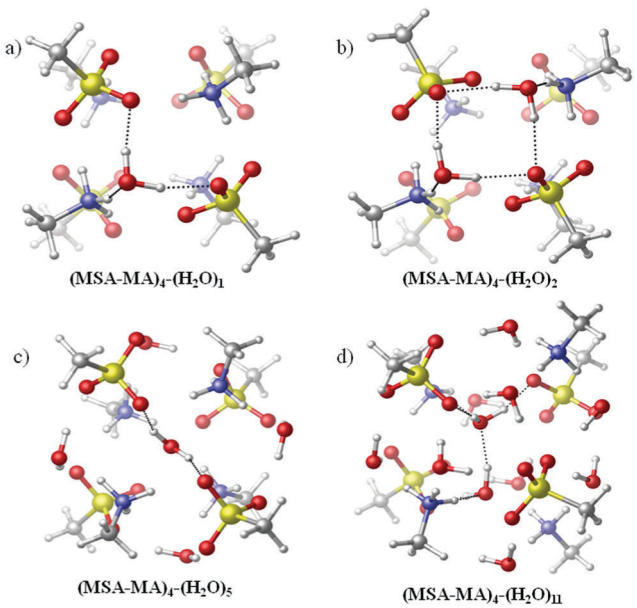

Fig. 2 Different types of locations for water: (a) one water on one face of the $(MSA–MA)_4$ unit; (b) two water molecules on the same face of the unit; (c) one water inside the unit; (d) two water molecules inside the unit.

second, it is located inside (Fig. 2c and d). Within the first type of structure, in the case of one water molecule (Fig. 2a), the water lies on one face of the $(MSA–MA)_4$ initial anhydrous unit. Under those conditions, water breaks one original hydrogen bond between MSA^- and H^+MA, and forms three new hydrogen bonds with two MSA^- and one H^+MA. Due to the strong ion-dipole forces between the cation and water, and the anion and water, H_2O becomes a strong bridge between the two ions, and no dissociation takes place. As seen in Fig. 2b, there are cases where two water molecules are located on the same face. As in the case of one water (Fig. 2a), the two water molecules insert themselves between two ion pairs on one face, and form a four-membered ring with two oxygen atoms of MSA^-. The addition of the second H_2O leads to a higher symmetry than for n = 1, which is also supported by the calculated free energies in Table 1 discussed in detail below.

In the second type of structure, water inserts itself inside the $(MSA–MA)_4$ initial unit. Fig. 2c shows one water molecule inside the unit, bonding with two MSA^-. Fig. 2d corresponds to two water molecules inside the unit. In this latter case, besides binding with MSA^- and H^+MA, the two water molecules located inside the unit connect with each other through one hydrogen bond.

Scheme 1 summarizes the different locations for water molecules, in which the sulfur and nitrogen atoms of the dry cluster are used to define the six faces of the cluster. For n = 1, 3 and 4, all the water molecules are located on separate faces of the $(MSA–MA)_4$ initial unit, and belong to the first type. For n = 2, the two water molecules lie on the same face. The $(MSA–MA)_4–(H_2O)_2$ cluster with the two water molecules located on separate faces exists as well, but it has about 1 kcal mol^{-1} higher energy (with zero-point energy correction) than the

Table 1 Dissociation energies with zero-point energy correction (ΔE) and Gibbs free energies (in kcal mol^{-1}) at 298 K (ΔG) of (MSA–MA)$_4$–(H$_2$O)$_n$, n = 0 to 12 clusters at the level of BLYP-D/6-31+G(d). Complete or partial dissociation into starting reactants are considered

	(MSA–MA)$_4$–(H$_2$O)$_n$ → 4MSA + 4MA + nH$_2$O		(MSA–MA)$_4$–(H$_2$O)$_n$ → (MSA–MA)$_4$ + nH$_2$O	
	$\Delta E1$	$\Delta G1$	$\Delta E2$	$\Delta G2$
n = 1	190.6	98.80	13.84	0.58
n = 2	205.2	104.1	28.39	5.83
n = 3	218.0	107.0	41.22	8.79
n = 4	230.7	110.4	53.96	12.18
n = 5	243.1	111.7	66.32	13.47
n = 6	255.8	115.9	79.02	17.70
n = 7	270.3	120.4	93.56	22.21
n = 8	280.0	118.6	103.3	20.47
n = 9	292.9	124.2	116.2	26.01
n = 10	303.8	124.3	127.0	26.12
n = 11	314.4	126.6	137.6	28.42
n = 12	326.6	128.6	149.9	30.37

a)

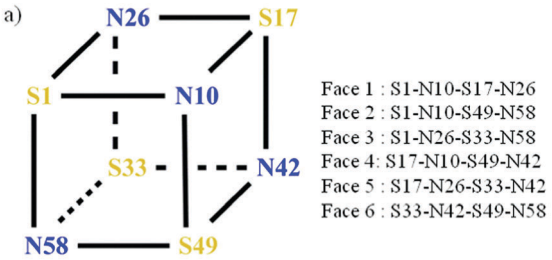

b)

Number of water molecules	Locations of the water
n=1	**1** (F3)
n=2	**2**(F3)
n=3	**1**(F3), **1**(F4), **1**(F6)
n=4	**1**(F2), **1**(F3), **1**(F4), **1**(F5)
n=5	**1**(F2), **1**(F3), **1**(F4), **1**(F5), **In1**
n=6	**1**(F1), **1**(F2), **1**(F3), **1**(F4), **1**(F5), **In1**
n=7	**1**(F1), **1**(F2), **1**(F3), **1**(F4), **1**(F5), **1**(F6), **In1**
n=8	**1**(F1), **2**(F3), **2**(F4), **2**(F6), **In1**
n=9	**2**(F1), **2**(F3), **2**(F4), **1**(F5), **1**(F6), **In1**
n=10	**2**(F1), **2**(F3), **2**(F4), **1**(F2), **1**(F5), **1**(F6), **In1**
n=11	**2**(F1), **2**(F3), **2**(F4), **1**(F2), **1**(F5), **1**(F6), **In2**
n=12	**2**(F1), **2**(F3), **2**(F4), **2**(F6), **1**(F2), **1**(F5), **In2**

Scheme 1 (a) The key skeleton of (MSA–MA)$_4$ with the sulfur (S) and nitrogen (N) atoms labeled along with the six defined faces; (b) locations of water in each system. *F*(*x*) means the "*x*th" face. **1** means only one water on one face; **2** means two water on one face; **In1** and **In2** mean one or two internal water, respectively.

structure with the two water molecules located on the same face. From n = 5 to n = 10, there is always one water inside the (MSA–MA)$_4$ unit binding with two MSA$^-$, while other water molecules are located on the faces of the unit. The water molecules on the faces also prefer to remain isolated (one water molecule per face); the situation where the cluster has two water molecules on one face is not observed until n = 8. For the case of n = 11 and 12, a second water molecule is incorporated inside the (MSA–MA)$_4$ unit cell, *i.e.*, the structure with the two internal water molecules has the lowest energy.

In short, in (MSA–MA)$_4$–(H$_2$O)$_n$, n = 1 to 12, most of the absorbed water molecules are around the initial (MSA–MA)$_4$ unit; with 5 to 10 water molecules, there is one water molecule incorporated inside the unit, and two water molecules that are internal for n = 11 and 12.

Thermodynamic stabilities

In order to verify the thermodynamic stabilities of the (MSA–MA)$_4$–(H$_2$O)$_n$, n = 1 to 12 clusters, the dissociation energies corrected with zero-point energy and Gibbs free energies (T = 298 K) for the twelve systems described above were calculated at the BLYP-D/6-31+G(d) level. The energies are listed in Table 1. We considered two possible paths. First, the clusters dissociate to four MSA monomers, four MA monomers and water, *i.e.*, (MSA–MA)$_4$–(H$_2$O)$_n$ → 4MSA + 4MA + nH$_2$O. From Table 1, the dissociation energy and free energy of each system in this reaction are quite high, *i.e.*, 190.6 to 326.6 kcal mol^{-1} for ΔE and 98.80 to 128.6 kcal mol^{-1} for ΔG. These positive values indicate that the dissociation process is highly endothermic. For the anhydrous cluster (MSA–MA)$_4$, the corresponding values are 176.8 kcal mol^{-1} for ΔE and 98.21 kcal mol^{-1} for ΔG respectively at the same level of theory. Considering (MSA–MA)$_4$ is a very stable cluster, the second dissociating pathway corresponding to the loss of water (dehydration), *i.e.*, (MSA–MA)$_4$–(H$_2$O)$_n$ → (MSA–MA)$_4$ + nH$_2$O, was also calculated. Similar to the first path, all the dissociation energies and Gibbs free energies (13.84 to 149.9 kcal mol^{-1} for ΔE and 0.58 to 30.37 kcal mol^{-1} for ΔG) are positive, and both of them increase with increasing number of water molecules. Hence, based on these results, we found that (MSA–MA)$_4$–(H$_2$O)$_n$ clusters are very stable thermodynamically.

Dynamic stabilities

The dynamic stabilities of (MSA–MA)$_4$–(H$_2$O)$_n$ clusters were examined by BOMD simulations carried out at T = 300 K. Structures for each system taken at 10 ps from the dynamic simulations are shown in Fig. S4 (ESI†). Simulation results show that all the clusters keep the key skeleton although the structural parameters change slightly. The locations of the water molecules that were initially on faces or incorporated inside the unit do not change, but the interactions of several water molecules changed under the influence of the temperature. Here, clusters with n = 2, 9, 11 and 12 were chosen as the representative structures for the discussion. Fig. 3a (n = 2) and Fig. 3b (n = 9) represent the two types of changes that occur when two water molecules are initially located on the same face of the (MSA–MA)$_4$ unit: in one case, the two water molecules form a new hydrogen bond between them (Fig. 3a), and on the other, one of the water breaks the initial hydrogen bond and now only connects with one MSA$^-$ (Fig. 3b). For n = 11 (Fig. 3c) and n = 12 (Fig. 3d) clusters, the change occurs on the second internal water molecule: instead of initially connecting with MSA$^-$ or H$^+$MA, the second internal water molecule forms new hydrogen bonds with other water molecules located on the faces. In

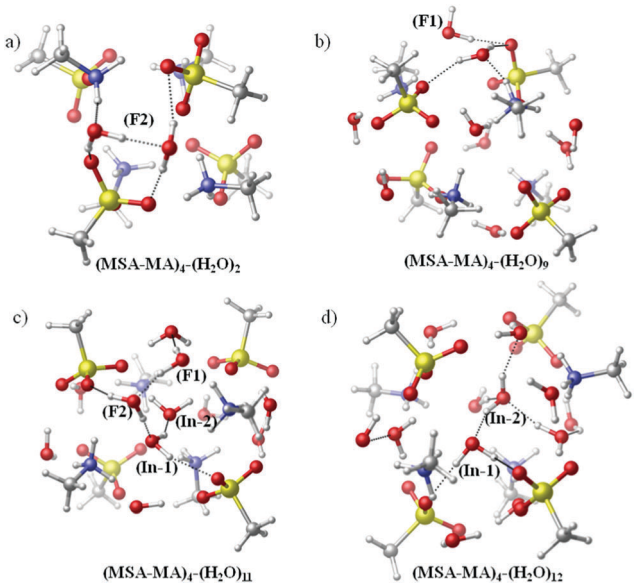

Fig. 3 Structures of $(MSA–MA)_4–(H_2O)_n$, n = 2, 9, 11 and 12 clusters at 10 ps from the dynamic simulations (T = 300 K) at the level of BLYP-D/6-31+G(d).

general, $(MSA–MA)_4–(H_2O)_n$, n = 1 to 12 clusters show good dynamic stability, and it is expected that at T = 300 K, water will still be taken up by $(MSA–MA)_4$ clusters.

Charge distributions in the hydrated clusters

In order to explore the effect of water on electronic properties, partial charges (δ) of $(MSA–MA)_4–(H_2O)_n$, n = 1 to 12 clusters were calculated using Natural Bond Orbital (NBO) analysis (see Table S1, ESI†). For the anhydrous cluster $(MSA–MA)_4$, the charge of each MSA^- fragment is −0.82 and it is 0.82 for each H^+MA fragment, which results from proton transfer from each MSA to each MA. Upon addition of water, the partial charges of MSA^- and H^+MA fragments only change slightly. The biggest charge difference is 0.04 for MSA^- (n = 7) and 0.06 for H^+MA (n = 9, 10, 12). The charge of each water lying on the face of the $(MSA–MA)_4$ unit is small, but positive (δ = 0.00–0.04). However, the internal water molecules are very different. For the clusters with one internal water (n = 5 to 10), the charge of the internal water molecule is negative except for n = 10. With increasing numbers of water molecules, the negative charge of the internal water gradually increases until it becomes positive (δ = −0.06 for n = 5 and δ = 0.01 for n = 10). When there are two internal water molecules in the $(MSA–MA)_4$ cluster (n = 11 and 12), both positive and negative charges on the internal water molecules exist. Based on the partial charge of each water molecule, the water located on the faces of the $(MSA–MA)_4$ unit has a positive charge and acts as an electron donor like MA, and the internal water molecules which have a negative charge act as an electron acceptor like MSA. Hence, through considering the total charges of all the water molecules in each system, it can be seen that water mainly plays a role as an electron donor (δ_{total} = 0.01–0.17), and the only case where water acts as an electron acceptor is for n = 5 (δ_{total} = −0.02).

Effect of hydration on sizes

The effects of water on the key skeleton and the size of the hydrated clusters were also investigated. In order to examine quantitative changes in the key $(MSA–MA)_4$ skeleton, the root-mean-square deviation (RMSD) of the geometry of the $(MSA–MA)_4$ unit in each hydrated cluster was calculated. Fig. S5a (ESI†) represents the RMSD values of the whole $(MSA–MA)_4$ unit (in black) and the same units without all the CH_3 groups (in red). When only one water molecule is added, the change in geometry of the $(MSA–MA)_4$ cluster is small, and the RMSD value is 0.5. However, the differences increase with increasing numbers of water molecules. The RMSD value is about 0.8 for n = 2 to 8 and 1.3 for n = 8 to 12. When the rotation of CH_3 groups is not considered, similar trends were also obtained (red data points in Fig. S5a, ESI†).

In order to directly observe a change, the geometries of the $(MSA–MA)_4$ unit from all the systems described were overlaid as shown in Fig. S5b (ESI†). It clearly shows that every fragment moves, and these changes may also affect the sizes of each cluster. Scheme 2a shows the lengths of hydrated and anhydrous $(MSA–MA)_4$ clusters in X, Y and Z directions, and the calculated percentage change (%) of sizes from anhydrous $(MSA–MA)_4$ are shown in Scheme 2b. When n = 1 and 2, the sizes of clusters in three directions do not change except for n = 2, a change in size is noted in the Y direction (about −17%). From n = 3 to n = 5, all the sizes begin to decrease and the cluster with n = 5 has the smallest sizes (−19% for X, −23% for Y and −12% for Z). Then, when more water molecules are added (n = 6 to 12), the size of the clusters increases and the biggest increase is about 29% for n = 11 in the X direction. However, the final sizes at n = 12 increase by 17% for X, 16% for Y and 13% for Z. In summary, the addition of water does not change the sizes of the hydrated clusters very much, and in fact, the sizes decrease for n = 3, 4 and 5.

Hydrate distributions

In order to estimate the distribution of hydrated clusters under realistic experimental conditions, the concentrations of each cluster in steady state were simulated using the ACDC code. Fig. 4a shows the hydrate distributions of the clusters from n = 0 to n = 12 at 19% RH. From these results, the order of populations is n = 7 (≈59%) ≫ n = 4 (≈11%) > n = 0 (≈10%) > n = 2 (≈7%) > n = 3 (≈6%) > n = 6 (≈5%) > n = 5/9 (≈1%) > n = 1/8/10/11/12 (≈0%). It is clear that the hydrated cluster with seven water molecules dominates, and its concentration is much higher than the others. This is also supported by the evaporation rates of the hydrated clusters from a single water evaporation pathway shown in Fig. 4b. The difference of evaporation rates between n = 7 and n = 8 is four orders of magnitudes, which means that the n = 8 cluster easily evaporates back to the n = 7 cluster. A similar situation exists for n = 1, 5, 10. These clusters are also likely to lose one water molecule. The hydrated cluster distributions at RH = 19% and 300 K shows that clusters with n > 12 water are not significantly present. Therefore, the clusters studied in this paper, ranging from n = 1 up to n = 12, describe all the hydrated clusters that are relevant.

a)

n	X	Y	Z
n=0	10.2	10.2	9.65
n=1	10.5	10.2	9.82
n=2	10.5	8.48	9.72
n=3	10.0	9.57	8.61
n=4	8.98	9.30	8.79
n=5	8.31	7.84	8.53
n=6	11.1	10.0	8.68
n=7	10.8	9.89	10.4
n=8	10.9	10.1	9.82
n=9	11.2	11.3	9.92
n=10	12.15	9.44	9.80
n=11	13.15	11.16	10.86
n=12	11.98	11.81	10.96

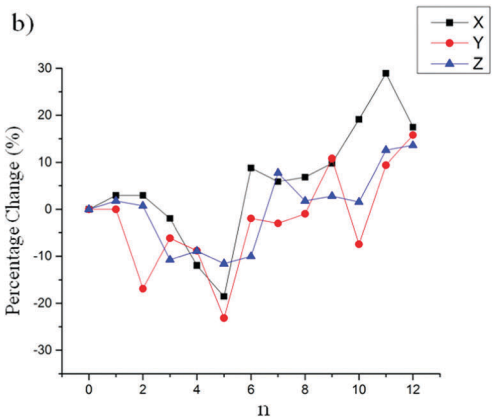

Scheme 2 (a) The lengths (Å) of $(MSA–MA)_4–(H_2O)_n$, n = 0 to 12 in X, Y and Z directions. (b) The percentage change (%) of the sizes of the different hydrated clusters compared to the anhydrous $(MSA–MA)_4$ cluster.

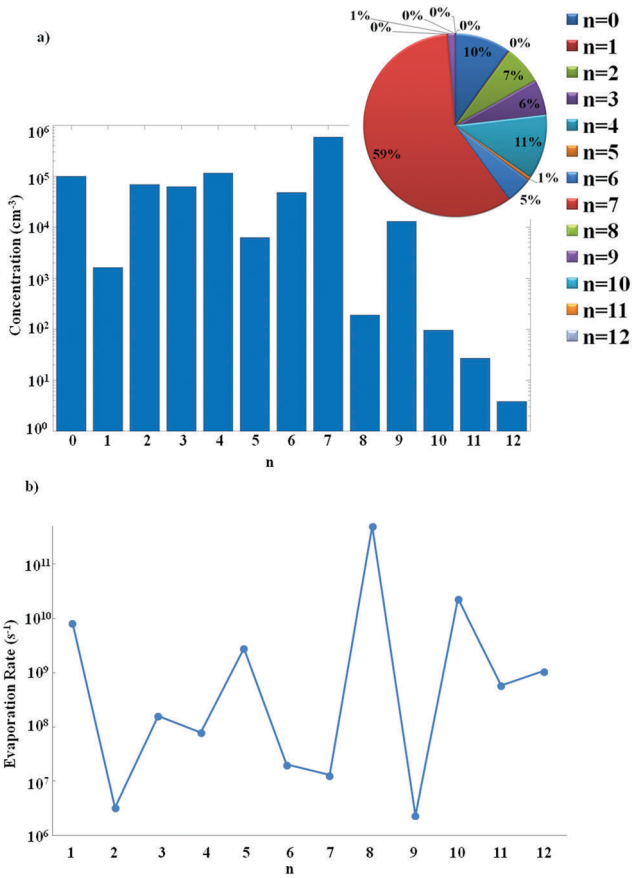

Fig. 4 (a) Hydrate distributions for $(MSA–MA)_4–(H_2O)_n$, n = 0 to 12 at 19% RH; (b) evaporation rates of the hydrated clusters from one single water evaporation pathway.

Experimental results

Experiments performed on this system are consistent with the results from quantum calculations described above. Fig. 5a shows the size distribution from the reaction of 6.9 ppb MSA (1.7×10^{11} molecules cm^{-3}) with 1.6 ppb MA (3.9×10^{10} molecules cm^{-3}) under dry and humid conditions where H_2O is added at a reaction time of 8.2 s after the formation of the MSA–MA particles. Under these conditions of excess MSA, the lifetime of MA is calculated to be ~50 ms, assuming a diffusion-controlled reaction. Thus, the 8.2 s of reaction time before water is added is more than sufficient for the MSA–MA reaction to be brought to completion. Under this configuration, no increase of detectable particles nor size change was observed at 19% RH ($[H_2O] = 1.5 \times 10^{17}$ molecules cm^{-3}) as reported in Table 2. Although the experiments were conducted with much more water than the theoretical calculations due to experimental constraints, the experiments show that the small stable (MSA–MA) particles are not impacted by the presence of water in agreement with the theoretical calculations presented in this study.

The absence of a deliquescence effect for the small systems studied here (~1 nm size for the theoretical calculations and ~3 nm for the experiments at a relative humidity of 19%) is not surprising. To the best of our knowledge, the deliquescence relative humidity (DRH) for the MSA–MA salt has not been reported, but previous studies have shown that sodium methanesulfonate deliquesced at about 70% DRH[84,85] while ammonium methanesulfonate showed a continuous uptake of water.[84] However, those measurements were all performed on ~1 μm particles deposited on a substrate, corresponding to a macroscopic thermodynamic bulk system. This may not hold for the small nanosize particles investigated here. Indeed, previous studies on hygroscopic growth and deliquescence for NaCl and $(NH_4)_2SO_4$ nanoparticles showed that at 100 nm, the DRH is not very different than that of the bulk value, but as the diameter of the particles approached only a few nm (8–15 nm), the relative humidity at which the particle deliquesced became systematically higher. In small nanosize systems, a large fraction of the molecules are on the surface rather than in the bulk and thus the surface energy becomes a significant term in the total free energy of the particle.

In a separate set of experiments, however, where water was introduced upstream (ring A, Fig. 5b) so that it was present *during* particle formation from MSA and MA, a very large increase of particles was observed (10 times more particles were detected) compared to the dry case. The particles were observed to be much larger as well, with a geometric mean

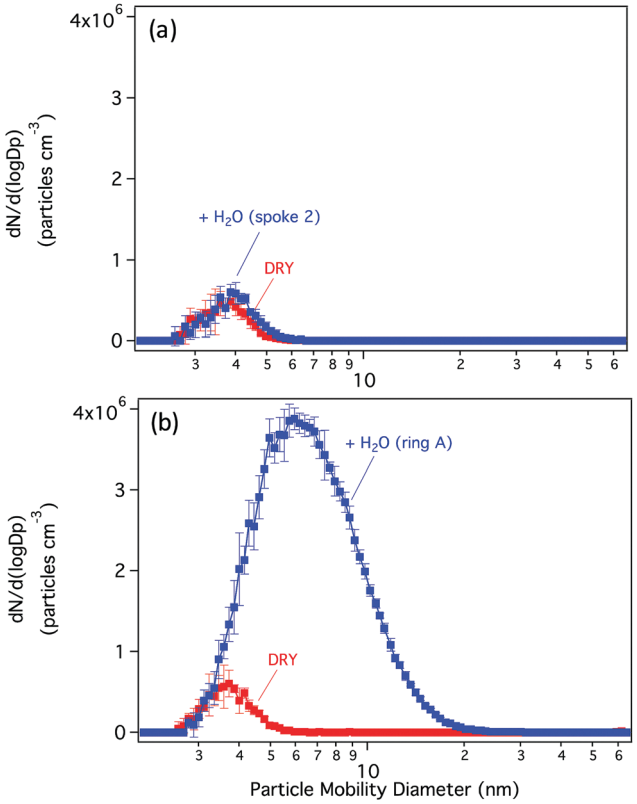

Fig. 5 Size distributions of particles from the reaction of 1.7×10^{11} MSA molecules cm^{-3} (6.9 ppb) with 3.9×10^{10} MA molecules cm^{-3} (1.6 ppb) measured by SMPS (a) under dry (red trace) conditions at a reaction time of 13.9 s, and in the presence of water vapor (RH ~ 18–19%; blue trace). In the latter case, the MSA and MA reacted for 8.2 s, and then interacted with water for an additional 5.7 s; (b) under dry (red trace) conditions at a reaction time of 13.9 s, and in the presence of water added at the first ring inlet (RH ~ 18–19%; blue trace) so that MSA, MA and H_2O were all present during particle formation. The size distributions are averages of five consecutive measurements and the error bars correspond to one standard deviation.

diameter of 6.5 nm compared to ~4 nm under dry conditions. Those results agree with our previous observations,[41,43] and indicate that water plays a central role in particle formation and growth in this system when all the reactants are present *at the same time*, despite the fact that the MSA reaction with water alone is not efficient. (A control experiment showed that less than 1 particle cm^{-3} was measured by the CPC for the reaction of MSA (ring B, 5.3 ppb) with H_2O (ring A, 19% RH) in the absence of MA, suggesting that the large number of particles is due to the presence of both the amine and water together.)

From a theoretical point of view, when 4MSA, 4MA and for example one water molecule interact at the same time, low energy level structures include 'unclosed' clusters. These clusters, as the one presented in Fig. S6 (ESI†), have a lot more opportunities to form hydrogen bonds with other species providing hooks to grow the initial cluster to larger sizes, consistent with the experimental observations.

The theoretical calculations cannot exactly replicate the conditions used for the experiments. The smallest particle size that can be detected and measured using the SMPS is 2.5 nm, which is much larger than the clusters calculated here. The time scales studied experimentally are also much larger than that can be addressed theoretically. Where interesting comparisons can be made, we investigated the connections between water uptake and increasing size, or in other words particle growth: the 1 nm theoretical model cluster can take up water without significant increase in size up to about $n \geq 6$. Beyond that size, the size of the particle continues to grow, and the increase becomes about 29% for $n = 11$. In the experiment, there is no significant uptake of water for the dry particles subsequently exposed to water vapor (19% RH), but for the particles produced with water vapor *at the same time* as the reactants, the size increases substantially compared to the dry case. Note that our experimental conditions had lower water vapor concentrations than found under many tropospheric conditions.

Conclusions

In this paper, the uptake of water by the MSA–MA nanoparticles *via* theoretical calculations and experiments was studied. It was shown that these hydrated nano-size clusters are thermodynamically stable at the level of BLYP-D/6-31+G(d). Loss of water and significant changes of structure do not take place for at least 10 ps throughout *ab initio* dynamic simulations. In the hydrated clusters, most of the water molecules lie on the face of the $(MSA–MA)_4$ initial dry unit, with water incorporated inside the initial unit when n ranges from five to twelve. Charge distributions in hydrated and anhydrous clusters are not very different. The sizes of the hydrated clusters differ by less than +29% to −25% in any dimension compared to the dry clusters, and the increased sizes are found when $n \geq 6$. From the hydrate distributions, the hydrated cluster with $n = 7$ dominates at 19% RH. Furthermore, the computed cluster distribution shows that the range of hydrated clusters studied, $n \leq 12$, encompasses

Table 2 Geometric mean diameter (nm) and total particle number concentration (# cm^{-3}) determined from size distribution measurements by SMPS

	Dry conditions[a]	Humid conditions (H_2O added at spoke 2)[b]	Humid conditions (H_2O added at ring A)[c]
Geometric mean diameter (nm)	3.7 (±0.1)	3.9 (±0.1)	6.5 (±0.04)
Total particle number conc. (# cm^{-3})	9.1 (±1.3) × 10^4	9.9 (±1.0) × 10^4	1.3 (±0.6) × 10^6

[a] Measurements were performed at a reaction time of 13.9 s (where $t = 0$ s corresponds to ring B); error bars correspond to one standard deviation from ten replicate measurements. [b] Measurements were performed after 8.2 s of reaction time between MSA and MA under dry conditions, and an additional 5.7 s of interaction of pre-formed particles with water (total reaction time = 13.9 s with $t = 0$ s corresponding to ring B); error bars correspond to one standard deviation from five replicate measurements. [c] Measurements were performed at a reaction time of 13.9 s (where $t = 0$ s corresponds to ring B); error bars correspond to one standard deviation from five replicate measurements.

all of the clusters present at significant concentrations under these conditions. In the experiments, the concentrations and size distributions of MSA–MA particles do not change when the particles formed under dry conditions are subsequently exposed to water vapor corresponding to 18–19% RH; however, drastic increases in both the size and number concentration are observed when all three reactants (MSA, MA and H_2O) are added simultaneously in the flow reactor. These results suggest that the effect of water on new particle formation and growth from MSA reactions with amines will be sensitive to whether water is present during the reaction, or added subsequently. Water is always present in the troposphere at significant concentrations, but not always in laboratory studies. Thus extrapolation of experiments under dry conditions to the atmosphere should be carried out with caution. Note that the theoretical calculations we studied in this paper focus on the small cluster with very limited numbers of water molecules. It will be very interesting in future studies to address the cluster with bulk water to compute the water loss rate by an approach based on Transition State Theory.

Conflicts of interest

There are no conflicts to declare.

Acknowledgements

The authors are grateful to the National Science Foundation (grant no. 1443140) for funding. Computational resources are the Green-planet cluster at University of California, Irvine. The authors thank the reviewer for pointing to us the dominant role of a specific cluster over a wide range of RH values. We thank Dr Nanna Myllys for her help in computing the hydrated cluster distribution and in providing useful insights.

References

1 J. H. Seinfeld and S. N. Pandis, *Atmospheric Chemistry and Physics: From Air Pollution to Climate Change*, Wiley-Interscience, Hoboken, N.J., 2nd edn, 2006.
2 T. F. Stocker, D. Qin, G. K. Plattner, M. Tignor, S. K. Allen, J. Boschung, A. Nauels, Y. Xia, B. Bex and B. M. Midgley, *IPCC, 2013: Climate Change 2013: The Physical Science Basis. Contribution of Working Group I to the Fifth Assessment Report of the Intergovernmental Panel on Climate Change*, Cambridge University Press, Cambridge, United Kingdom and New York, NY, USA, 2013.
3 C. A. Pope and D. W. Dockery, *J. Air Waste Manage. Assoc.*, 2006, **56**, 709–742.
4 J. L. Mauderly and J. C. Chow, *Inhalation Toxicol.*, 2008, **20**, 257–288.
5 J. Lelieveld, J. S. Evans, M. Fnais, D. Giannadaki and A. Pozzer, *Nature*, 2015, **525**, 367–371.
6 B. J. Finlayson-Pitts and J. N. Pitts Jr, *Chemistry of the Upper and Lower Atmosphere: Theory, Experiments, and Applications*, Academic Press, 1999.
7 R. Zhang, A. Khalizov, L. Wang, M. Hu and W. Xu, *Chem. Rev.*, 2012, **112**, 1957–2011.
8 S. T. Martin, *Chem. Rev.*, 2000, **100**, 3403–3454.
9 M. Kulmala, J. Kontkanen, H. Junninen, K. Lehtipalo, H. E. Manninen, T. Nieminen, T. Petäjä, M. Sipilä, S. Schobesberger, P. Rantala, A. Franchin, T. Jokinen, E. Järvinen, M. Äijälä, J. Kangasluoma, J. Hakala, P. P. Aalto, P. Paasonen, J. Mikkilä, J. Vanhanen, J. Aalto, H. Hakola, U. Makkonen, T. Ruuskanen, R. L. Mauldin, J. Duplissy, H. Vehkamäki, J. Bäck, A. Kortelainen, I. Riipinen, T. Kurtén, M. V. Johnston, J. N. Smith, M. Ehn, T. F. Mentel, K. E. J. Lehtinen, A. Laaksonen, V.-M. Kerminen and D. R. Worsnop, *Science*, 2013, **339**, 943–946.
10 M. Sipilä, T. Berndt, T. Petäjä, D. Brus, J. Vanhanen, F. Stratmann, J. Patokoski, R. L. Mauldin, A.-P. Hyvärinen, H. Lihavainen and M. Kulmala, *Science*, 2010, **327**, 1243–1246.
11 J. H. Zollner, W. A. Glasoe, B. Panta, K. K. Carlson, P. H. McMurry and D. R. Hanson, *Atmos. Chem. Phys.*, 2012, **12**, 4399–4411.
12 T. Berndt, F. Stratmann, M. Sipilä, J. Vanhanen, T. Petäjä, J. Mikkilä, A. Grüner, G. Spindler, R. Lee Mauldin III, J. Curtius, M. Kulmala and J. Heintzenberg, *Atmos. Chem. Phys.*, 2010, **10**, 7101–7116.
13 M. E. Erupe, A. A. Viggiano and S.-H. Lee, *Atmos. Chem. Phys.*, 2011, **11**, 4767–4775.
14 H. Yu, R. McGraw and S.-H. Lee, *Geophys. Res. Lett.*, 2012, **39**, L02807.
15 W. A. Glasoe, K. Volz, B. Panta, N. Freshour, R. Bachman, D. R. Hanson, P. H. McMurry and C. Jen, *J. Geophys. Res.: Atmos.*, 2015, **120**, 2014JD022730.
16 J. Almeida, S. Schobesberger, A. Kürten, I. K. Ortega, O. Kupiainen-Määttä, A. P. Praplan, A. Adamov, A. Amorim, F. Bianchi, M. Breitenlechner, A. David, J. Dommen, N. M. Donahue, A. Downard, E. Dunne, J. Duplissy, S. Ehrhart, R. C. Flagan, A. Franchin, R. Guida, J. Hakala, A. Hansel, M. Heinritzi, H. Henschel, T. Jokinen, H. Junninen, M. Kajos, J. Kangasluoma, H. Keskinen, A. Kupc, T. Kurtén, A. N. Kvashin, A. Laaksonen, K. Lehtipalo, M. Leiminger, J. Leppä, V. Loukonen, V. Makhmutov, S. Mathot, M. J. McGrath, T. Nieminen, T. Olenius, A. Onnela, T. Petäjä, F. Riccobono, I. Riipinen, M. Rissanen, L. Rondo, T. Ruuskanen, F. D. Santos, N. Sarnela, S. Schallhart, R. Schnitzhofer, J. H. Seinfeld, M. Simon, M. Sipilä, Y. Stozhkov, F. Stratmann, A. Tomé, J. Tröstl, G. Tsagkogeorgas, P. Vaattovaara, Y. Viisanen, A. Virtanen, A. Vrtala, P. E. Wagner, E. Weingartner, H. Wex, C. Williamson, D. Wimmer, P. Ye, T. Yli-Juuti, K. S. Carslaw, M. Kulmala, J. Curtius, U. Baltensperger, D. R. Worsnop, H. Vehkamäki and J. Kirkby, *Nature*, 2013, **502**, 359–363.
17 T. Kurtén, L. Torpo, C.-G. Ding, H. Vehkamäki, M. R. Sundberg, K. Laasonen and M. Kulmala, *J. Geophys. Res.: Atmos.*, 2007, **112**, D04210.
18 J. C. Ianni and A. R. Bandy, *J. Phys. Chem. A*, 1999, **103**, 2801–2811.
19 A. B. Nadykto, F. Yu, M. V. Jakovleva, J. Herb and Y. Xu, *Entropy*, 2011, **13**, 554–569.
20 H. Henschel, T. Kurtén and H. Vehkamäki, *J. Phys. Chem. A*, 2016, **120**, 1886–1896.

21 V. Loukonen, T. Kurtén, I. K. Ortega, H. Vehkamäki, A. A. H. Pádua, K. Sellegri and M. Kulmala, *Atmos. Chem. Phys.*, 2010, **10**, 4961–4974.
22 J. W. DePalma, D. J. Doren and M. V. Johnston, *J. Phys. Chem. A*, 2014, **118**, 5464–5473.
23 D. J. Bustos, B. Temelso and G. C. Shields, *J. Phys. Chem. A*, 2014, **118**, 7430–7441.
24 K. E. Anderson, J. I. Siepmann, P. H. McMurry and J. VandeVondele, *J. Am. Chem. Soc.*, 2008, **130**, 14144–14147.
25 D. S. Lambrecht, L. McCaslin, S. S. Xantheas, E. Epifanovsky and M. Head-Gordon, *Mol. Phys.*, 2012, **110**, 2513–2521.
26 S. M. Kreidenweis and J. H. Seinfeld, *Atmos. Environ. (1967)*, 1988, **22**, 283–296.
27 M. C. Facchini, S. Decesari, M. Rinaldi, C. Carbone, E. Finessi, M. Mircea, S. Fuzzi, F. Moretti, E. Tagliavini, D. Ceburnis and C. D. O'Dowd, *Environ. Sci. Technol.*, 2008, **42**, 9116–9121.
28 R. J. Hopkins, Y. Desyaterik, A. V. Tivanski, R. A. Zaveri, C. M. Berkowitz, T. Tyliszczak, M. K. Gilles and A. Laskin, *J. Geophys. Res.: Atmos.*, 2008, **113**, D04209.
29 B. E. Wyslouzil, J. H. Seinfeld and R. C. Flagan, *J. Chem. Phys.*, 1991, **94**, 6827–6841.
30 B. E. Wyslouzil, J. H. Seinfeld, R. C. Flagan and K. Okuyama, *J. Chem. Phys.*, 1991, **94**, 6842–6850.
31 S. M. Kreidenweis, R. C. Flagan, J. H. Seinfeld and K. Okuyama, *J. Aerosol Sci.*, 1989, **20**, 585–607.
32 V.-M. Kerminen, M. Aurela, R. E. Hillamo and A. Virkkula, *Tellus B*, 1997, **49**, 159–171.
33 V. Perraud, J. R. Horne, A. S. Martinez, J. Kalinowski, S. Meinardi, M. L. Dawson, L. M. Wingen, D. Dabdub, D. R. Blake, R. B. Gerber and B. J. Finlayson-Pitts, *Proc. Natl. Acad. Sci. U. S. A.*, 2015, **112**, 13514–13519.
34 A. Sorooshian, L. T. Padró, A. Nenes, G. Feingold, A. McComiskey, S. P. Hersey, H. Gates, H. H. Jonsson, S. D. Miller, G. L. Stephens, R. C. Flagan and J. H. Seinfeld, *Global Biogeochem. Cycles*, 2009, **23**, GB4007.
35 C. J. Gaston, K. A. Pratt, X. Qin and K. A. Prather, *Environ. Sci. Technol.*, 2010, **44**, 1566–1572.
36 H. Bardouki, H. Berresheim, M. Vrekoussis, J. Sciare, G. Kouvarakis, K. Oikonomou, J. Schneider and N. Mihalopoulos, *Atmos. Chem. Phys.*, 2003, **3**, 1871–1886.
37 H. Berresheim, T. Elste, H. G. Tremmel, A. G. Allen, H.-C. Hansson, K. Rosman, M. Dal Maso, J. M. Mäkelä, M. Kulmala and C. D. O'Dowd, *J. Geophys. Res.: Atmos.*, 2002, PAR 5-1.
38 F. L. Eisele and D. J. Tanner, *J. Geophys. Res.: Atmos.*, 1993, **98**, 9001–9010.
39 M. L. Dawson, M. E. Varner, V. Perraud, M. J. Ezell, R. B. Gerber and B. J. Finlayson-Pitts, *Proc. Natl. Acad. Sci. U. S. A.*, 2012, **109**, 18719–18724.
40 H. Chen, M. J. Ezell, K. D. Arquero, M. E. Varner, M. L. Dawson, R. B. Gerber and B. J. Finlayson-Pitts, *Phys. Chem. Chem. Phys.*, 2015, **17**, 13699–13709.
41 H. Chen, M. E. Varner, R. B. Gerber and B. J. Finlayson-Pitts, *J. Phys. Chem. B*, 2016, **120**, 1526–1536.
42 K. D. Arquero, J. Xu, R. B. Gerber and B. J. Finlayson-Pitts, *Phys. Chem. Chem. Phys.*, 2017, **19**, 28286–28301.
43 K. D. Arquero, R. B. Gerber and B. J. Finlayson-Pitts, *Environ. Sci. Technol.*, 2017, **51**, 2124–2130.
44 H. Chen and B. J. Finlayson-Pitts, *Environ. Sci. Technol.*, 2017, **51**, 243–252.
45 M. L. Dawson, M. E. Varner, V. Perraud, M. J. Ezell, J. Wilson, A. Zelenyuk, R. B. Gerber and B. J. Finlayson-Pitts, *J. Phys. Chem. C*, 2014, **118**, 29431–29440.
46 S. Li, L. Zhang, W. Qin and F.-M. Tao, *Chem. Phys. Lett.*, 2007, **447**, 33–38.
47 J. Xu, B. J. Finlayson-Pitts and R. B. Gerber, *J. Phys. Chem. A*, 2017, **121**, 2377–2385.
48 J. Xu, B. J. Finlayson-Pitts and R. B. Gerber, *Phys. Chem. Chem. Phys.*, 2017, **19**, 31949–31957.
49 N. Bork, J. Elm, T. Olenius and H. Vehkamäki, *Atmos. Chem. Phys.*, 2014, **14**, 12023–12030.
50 H. Zhao, X. Jiang and L. Du, *Chemosphere*, 2017, **174**, 689–699.
51 M. Kumar and J. S. Francisco, *Proc. Natl. Acad. Sci. U. S. A.*, 2017, **114**, 12401–12406.
52 L. Wang, *J. Phys. Chem. A*, 2007, **111**, 3642–3651.
53 S.-K. Miao, S. Jiang, X.-Q. Peng, Y.-R. Liu, Y.-J. Feng, Y.-B. Wang, F. Zhao, T. Huang and W. Huang, *RSC Adv.*, 2018, **8**, 3250–3263.
54 A. Givan, A. Loewenschuss and C. J. Nielsen, *J. Mol. Struct.*, 2005, **748**, 77–90.
55 T. Berndt, M. Sipilä, F. Stratmann, T. Petäjä, J. Vanhanen, J. Mikkilä, J. Patokoski, R. Taipale, R. L. Mauldin III and M. Kulmala, *Atmos. Chem. Phys.*, 2014, **14**, 751–764.
56 M. Kulmala, H. Vehkamäki, T. Petäjä, M. Dal Maso, A. Lauri, V.-M. Kerminen, W. Birmili and P. H. McMurry, *J. Aerosol Sci.*, 2004, **35**, 143–176.
57 D. G. Imre, J. Xu, I. N. Tang and R. McGraw, *J. Phys. Chem. A*, 1997, **101**, 4191–4195.
58 I. K. Ortega, O. Kupiainen, T. Kurtén, T. Olenius, O. Wilkman, M. J. McGrath, V. Loukonen and H. Vehkamäki, *Atmos. Chem. Phys.*, 2012, **12**, 225–235.
59 H. Henschel, T. Kurtén and H. Vehkamäki, *J. Phys. Chem. A*, 2016, **120**, 1886–1896.
60 N. T. Tsona, H. Henschel, N. Bork, V. Loukonen and H. Vehkamäki, *J. Phys. Chem. A*, 2015, **119**, 9670–9679.
61 H. Henschel, J. C. A. Navarro, T. Yli-Juuti, O. Kupiainen-Määttä, T. Olenius, I. K. Ortega, S. L. Clegg, T. Kurtén, I. Riipinen and H. Vehkamäki, *J. Phys. Chem. A*, 2014, **118**, 2599–2611.
62 K. H. Weber, Q. Liu and F.-M. Tao, *J. Phys. Chem. A*, 2014, **118**, 1451–1468.
63 X.-Q. Peng, T. Huang, S.-K. Miao, J. Chen, H. Wen, Y.-J. Feng, Y. Hong, C.-Y. Wang and W. Huang, *RSC Adv.*, 2016, **6**, 46582–46593.
64 S.-S. Lv, S.-K. Miao, Y. Ma, M.-M. Zhang, Y. Wen, C.-Y. Wang, Y.-P. Zhu and W. Huang, *J. Phys. Chem. A*, 2015, **119**, 8657–8666.
65 L. J. Larson, A. Largent and F.-M. Tao, *J. Phys. Chem. A*, 1999, **103**, 6786–6792.
66 L. J. Larson, M. Kuno and F.-M. Tao, *J. Chem. Phys.*, 2000, **112**, 8830–8838.
67 X. Ge, A. S. Wexler and S. L. Clegg, *Atmos. Environ.*, 2011, **45**, 524–546.

68 Y. You, V. P. Kanawade, J. A. de Gouw, A. B. Guenther, S. Madronich, M. R. Sierra-Hernández, M. Lawler, J. N. Smith, S. Takahama, G. Ruggeri, A. Koss, K. Olson, K. Baumann, R. J. Weber, A. Nenes, H. Guo, E. S. Edgerton, L. Porcelli, W. H. Brune, A. H. Goldstein and S.-H. Lee, *Atmos. Chem. Phys.*, 2014, **14**, 12181–12194.
69 I.-H. Chang, C.-G. Lee and D. S. Lee, *Anal. Chem.*, 2003, **75**, 6141–6146.
70 C. Lee, W. Yang and R. G. Parr, *Phys. Rev. B: Condens. Matter Mater. Phys.*, 1988, **37**, 785–789.
71 S. Grimme, J. Antony, S. Ehrlich and H. Krieg, *J. Chem. Phys.*, 2010, **132**, 154104.
72 G. A. Petersson, A. Bennett, T. G. Tensfeldt, M. A. Al-Laham, W. A. Shirley and J. Mantzaris, *J. Chem. Phys.*, 1988, **89**, 2193–2218.
73 G. A. Petersson and M. A. Al-Laham, *J. Chem. Phys.*, 1991, **94**, 6081–6090.
74 T. H. Dunning Jr, *J. Chem. Phys.*, 1989, **90**, 1007–1023.
75 R. Krishnan, J. S. Binkley, R. Seeger and J. A. Pople, *J. Chem. Phys.*, 1980, **72**, 650–654.
76 A. D. Becke, *J. Chem. Phys.*, 1993, **98**, 5648–5652.
77 R. G. Parr and Y. Weitao, *Density-Functional Theory of Atoms and Molecules*, Oxford University Press, 1994.
78 A. E. Reed and F. Weinhold, *J. Chem. Phys.*, 1983, **78**, 4066–4073.
79 J. P. Foster and F. Weinhold, *J. Am. Chem. Soc.*, 1980, **102**, 7211–7218.
80 Y. Shao, Z. Gan, E. Epifanovsky, A. T. B. Gilbert, M. Wormit, J. Kussmann, A. W. Lange, A. Behn, J. Deng, X. Feng, D. Ghosh, M. Goldey, P. R. Horn, L. D. Jacobson, I. Kaliman, R. Z. Khaliullin, T. Kuś, A. Landau, J. Liu, E. I. Proynov, Y. M. Rhee, R. M. Richard, M. A. Rohrdanz, R. P. Steele, E. J. Sundstrom, H. L. Woodcock III, P. M. Zimmerman, D. Zuev, B. Albrecht, E. Alguire, B. Austin, G. J. O. Beran, Y. A. Bernard, E. Berquist, K. Brandhorst, K. B. Bravaya, S. T. Brown, D. Casanova, C.-M. Chang, Y. Chen, S. H. Chien, K. D. Closser, D. L. Crittenden, M. Diedenhofen, R. A. DiStasio Jr, H. Do, A. D. Dutoi, R. G. Edgar, S. Fatehi, L. Fusti-Molnar, A. Ghysels, A. Golubeva-Zadorozhnaya, J. Gomes, M. W. D. Hanson-Heine, P. H. P. Harbach, A. W. Hauser, E. G. Hohenstein, Z. C. Holden, T.-C. Jagau, H. Ji, B. Kaduk, K. Khistyaev, J. Kim, J. Kim, R. A. King, P. Klunzinger, D. Kosenkov, T. Kowalczyk, C. M. Krauter, K. U. Lao, A. D. Laurent, K. V. Lawler, S. V. Levchenko, C. Y. Lin, F. Liu, E. Livshits, R. C. Lochan, A. Luenser, P. Manohar, S. F. Manzer, S.-P. Mao, N. Mardirossian, A. V. Marenich, S. A. Maurer, N. J. Mayhall, E. Neuscamman, C. M. Oana, R. Olivares-Amaya, D. P. O'Neill, J. A. Parkhill, T. M. Perrine, R. Peverati, A. Prociuk, D. R. Rehn, E. Rosta, N. J. Russ, S. M. Sharada, S. Sharma, D. W. Small, A. Sodt, T. Stein, D. Stück, Y.-C. Su, A. J. W. Thom, T. Tsuchimochi, V. Vanovschi, L. Vogt, O. Vydrov, T. Wang, M. A. Watson, J. Wenzel, A. White, C. F. Williams, J. Yang, S. Yeganeh, S. R. Yost, Z.-Q. You, I. Y. Zhang, X. Zhang, Y. Zhao, B. R. Brooks, G. K. L. Chan, D. M. Chipman, C. J. Cramer, W. A. Goddard III, M. S. Gordon, W. J. Hehre, A. Klamt, H. F. Schaefer III, M. W. Schmidt, C. D. Sherrill, D. G. Truhlar, A. Warshel, X. Xu, A. Aspuru-Guzik, R. Baer, A. T. Bell, N. A. Besley, J.-D. Chai, A. Dreuw, B. D. Dunietz, T. R. Furlani, S. R. Gwaltney, C.-P. Hsu, Y. Jung, J. Kong, D. S. Lambrecht, W. Liang, C. Ochsenfeld, V. A. Rassolov, L. V. Slipchenko, J. E. Subotnik, T. V. Voorhis, J. M. Herbert, A. I. Krylov, P. M. W. Gill and M. Head-Gordon, *Mol. Phys.*, 2015, **113**, 184–215.
81 M. J. McGrath, T. Olenius, I. K. Ortega, V. Loukonen, P. Paasonen, T. Kurtén, M. Kulmala and H. Vehkamäki, *Atmos. Chem. Phys.*, 2012, **12**, 2345–2355.
82 M. J. Ezell, H. Chen, K. D. Arquero and B. J. Finlayson-Pitts, *J. Aerosol Sci.*, 2014, **78**, 30–40.
83 M. L. Dawson, V. Perraud, A. Gomez, K. D. Arquero, M. J. Ezell and B. J. Finlayson-Pitts, *Atmos. Meas. Tech.*, 2014, **7**, 2733–2744.
84 Y. Liu and A. Laskin, *J. Phys. Chem. A*, 2009, **113**, 1531–1538.
85 G. Zeng, J. Kelley, J. D. Kish and Y. Liu, *J. Phys. Chem. A*, 2014, **118**, 583–591.